

Dynamical evolution of hadronic matter in relativistic collisions

D. J. Dean,^{1,3} A. S. Umar,^{2,1} and M. R. Strayer¹

¹*Center for Computationally Intensive Physics, Physics Division, Oak Ridge National Laboratory, Oak Ridge, Tennessee 37831*

²*Vanderbilt University, Department of Physics & Astronomy, Nashville, Tennessee 37235*

³*W. K. Kellogg Radiation Laboratory, California Institute of Technology, Pasadena, California 91125*

(Received 19 April 1993)

We use the (3+1)-dimensional string-parton model to study relativistic collisions of heavy ions at CERN energies. Various inclusive hadronic observables, such as transverse energy, $dE_T/d\eta$, and rapidity distributions, are calculated and compared with WA80 and NA35 data. We study secondary interactions that occur during the dynamical evolution, and show that these interactions tend to fill the midrapidity region. The dynamical evolution of the energy density of produced mesons and their thermodynamic properties are also studied.

PACS number(s): 25.75.+r, 12.38.Mh

I. INTRODUCTION

Relativistic heavy-ion collisions offer the opportunity to study highly excited hadronic matter in the laboratory as it evolves in space-time. Depending on the number and energy density of the produced particles, the highly excited matter may form a quark-gluon plasma in which there are no identifiable hadronic states [1]. However it is becoming increasingly apparent that identification of this novel form of matter is experimentally a very difficult task [1]. The study of the transition from excited hadronic matter to the quark-gluon plasma is a difficult theoretical undertaking as well. A number of finite-temperature lattice gauge calculations, including dynamical fermions, have been performed to determine the nature of the phase transition to the quark-gluon plasma [2], and to study the properties of the plasma [3]. Earlier calculations on coarse lattices suggested a first-order chiral phase transition from hadronic to quark matter [2]. However, recent refined calculations with two and three dynamical quarks seem to question such a phase transition [4] for realistic quark masses. Other work indicates that there is a maximum hadron temperature $(T_H)_{\max}$ and a minimum perturbative quark-gluon temperature $(T_{QG})_{\min}$, such that $(T_{QG})_{\min} > (T_H)_{\max}$, and therefore there is no common temperature at which hadron and quark-gluon plasma equilibrium states can coexist [5]. The difficulty of detecting the quark-gluon plasma formation is mostly due to the confining nature of the strong interaction, which only allows hadronic final states, and thus a detailed understanding of all of the hadronic decay processes is necessary before the identification of the plasma can be achieved. Many possible experimental signatures have been suggested that would indicate the existence of the plasma state, yet none of these is able to stand alone as the definitive signal. Indeed, observed phenomena such as J/ψ suppression [6], enhanced production of strange hadrons [7], and increased transverse momenta of emitted particles [8], although experimentally observed, do not conclusively indicate plasma formation [9].

Various models have been developed to address the ordinary hadronic physics that occurs in relativistic heavy-ion collisions. These include string-based fragmentation models such as the LUND model [10], and its extensions in FRITIOF [11], which assume that excited hadrons behave as a chain of color dipoles that move like one-dimensional relativistic strings. Interactions are introduced via multiple small momentum exchanges between the color dipoles of two overlapping strings. Other non-dynamical models are the dual-parton model [12], in which the strings are formed by soft gluon exchange between the valence partons of the colliding hadrons. The quark-gluon string model (QGSM) [13], also based on the dual-parton model, has been developed to study soft parton collisions, and includes rescattering. The *strings* in the above models are in fact one-dimensional constructions in momentum space, and string evolution is carried out in this space. They are sometimes referred to as the longitudinal phase-space models. Any coordinate space quantities that these models may study come from transformations from momentum space one-dimensional string coordinates to configuration space. Relativistic quantum molecular dynamics (RQMD) calculations have also been performed to study relativistic collision phenomena [14]. This approach combines resonance formation and decay of light hadronic states, and one-dimensional string fragmentation (LUND model) for very heavy resonances. RQMD follows the full space-time evolution of the light hadronic states, and uses one-dimensional momentum space evolution for the heavy states via the LUND string description.

Space-time models have also been developed to study the plasma phase. Hydrodynamic and fluid dynamic models have been used to describe the collision phenomena [15] from the point of view of a relativistic one-fluid plasma. These calculations assume an initial excited state and follow the fluid flow thereafter. Similarly, time-dependent parton cascades [16] are used to study the plasma phase. The parton cascade model assumes that all initial nucleons in a nucleus may be resolved into their parton distributions. Interactions occur through pertur-

bative $2 \rightarrow 2$ QCD processes, and hadronization takes place through parton fragmentation and recombination.

Recently, we have developed a real-time dynamical model for studying the inclusive properties of hadronic collisions in three dimensions [17–20]. The model is based on the Nambu-Gotō string description of hadrons supplemented by extensions to incorporate the basic features of the parton model, together with a hadronization mechanism. The advantage of having a fully dynamical model is the possibility to explore the detailed time evolution of the hadronic matter. Furthermore, since the model is fully three dimensional, all of the transverse degrees of freedom are available to the evolving system. Further details of the model are mentioned below. The model has been successfully applied to the study of high-energy e^+e^- , pp [17], μp , and μA [18,19] collisions. These calculations have been used to fix all of the parameters present in the model. This paper is an application of the model to the study of relativistic nucleus-nucleus collisions. For all of the calculations presented here, the model parameters have been held fixed at their previously determined values.

The paper is organized as follows. In Sec. II we give a brief outline of the string parton model. In Sec. III we apply the string-parton model to various nucleus-nucleus collisions and compare our results to WA80 [21] and NA35 [22] data. Having shown that the model successfully reproduces the average hadronic experimental data, we turn to calculations that explore the underlying dynamics of the relativistic collisions. In Secs. IV and V we discuss the dynamical energy densities and the thermodynamic properties of the produced particles, respectively. We conclude this paper in Sec. VI with a discussion of our results.

II. STRING-PARTON MODEL FORMALISM

Classical strings serve as a phenomenological tool to study the physics of extended confined objects [23]. The derivation of the string equations of motion is considerably involved, and has been discussed previously [17]. Here we will outline some of the basic features of the model (we work in natural units where $\hbar = c = 1$).

Nambu strings sweep out a two-dimensional hypersurface in the (3+1)-dimensional space-time. The invariant area swept by the string is used to write the action integral for the string motion [17] by introducing a constant string tension κ . The variation of the action yields the equations of motion for the strings together with the appropriate boundary conditions. The string motion can be exclusively written in light-cone coordinates of the string end points [23]. For a string at rest, massless end points move at the speed of light along the string. The total string invariant mass, which is determined by the initial particle mass and the boosts, is a constant of the motion.

In building the phenomenology of the dynamical string-parton model description of relativistic heavy-ion collisions, it is desirable to start from a description which entails many of the features observed for elementary high-energy processes. One of the most important proper-

ties of hadrons is their substructure observed mainly via deep-inelastic charged lepton-hadron collisions [24,25]. The common feature of the high-energy data is the Q^2 (four-momentum transfer) independence of the structure functions for fixed values of the variable $x = Q^2/2M\nu$, where M denotes the nucleon mass and ν is the transferred energy. In the parton model this scaling behavior is explained in terms of the presence of pointlike charged constituents generically called partons. It can be shown in the infinite momentum frame that the scaling variable x is the fraction of the momentum of the nucleon carried by the struck parton. This relation is true only in this frame; however, it is approximately valid in other frames, if the partons are assumed to be massless. Corrections arising from the finite parton mass are usually neglected, as well as the small differences between neutron and proton distribution functions [26]. The string-parton model reproduces the observed structure functions by utilizing the end-point dynamics of strings; at any given instant the energy and momentum is shared by the string segment (string shrinks or stretches) and the end points. This allows the natural identification of these end points as partons belonging to the hadron described by the entire string. This identification was first used in the string-parton model to establish a connection between strings and parton structure functions. For the description of baryons, one end represents a single quark whereas the other end a diquark. Each quark carries a baryon number of $1/3$ thus giving $B = 1$ for baryons. The description of mesons involves a quark at one end, and an antiquark at the other. In the case of a longitudinal string in its rest frame, two end points carry the same amount of energy, which for a rest mass M and instantaneous length L is

$$E_q = \frac{M - \kappa L}{2}. \quad (2.1)$$

Thus, for relativistic strings at rest, it is natural to define a fractional momentum variable associated with the string end points. Assuming collinear motion along the z direction, which will be the boost axis, we define the string longitudinal momentum fraction in terms of the ratio of the light-cone variables,

$$x_s = \frac{k_0 + k_3}{P_0 + P_3}, \quad (2.2)$$

where k is the end-point four-momentum and P is the total string four-momentum. The variable x_s is Lorentz invariant for boosts in the longitudinal direction. We have shown in Ref. [17] that different dynamical states of motion of the strings give rise to different fractional momentum distributions of the string end points, which are identified as massless partons. An ensemble average of different dynamical states of the strings accurately reproduces the valence quark structure function of the proton [17].

The initial setup of a nuclear collision is done as follows: nuclei are randomly generated within an impact parameter range by employing a Fermi-density distribution

$$\rho(r) = \frac{\rho_0}{1 + \exp[(r - c)/a_0]}, \quad (2.3)$$

where a_0 is the thickness of the nuclear surface, c is the half-density radius, and ρ_0 is the central density. The numerical values of c and a_0 are found by computing the charge radius and mass $\rho(r)$ of each nucleus. The nuclear volume is then populated with nucleons, simulated by strings, such that no two nucleons overlap in the initial state. Each nucleon is initialized according to a Monte Carlo sampling of the strings so as to reproduce the correct parton distribution functions, as described above. The nuclear impact parameter, b , may be fixed at a particular value, or given a range, and is distributed as $2\pi b db$. The two nuclei are then boosted with the collision γ , and the time evolution proceeds via the string equations of motion.

In order to simulate hadron-hadron collisions, the strings must interact with each other. This interaction mechanism should lead to excited strings which must then decay via a suitable hadronization mechanism. An assumption is made in the string-parton model, namely that the final state interactions, which confine the partons, act at large space-time distances of the order of the hadron size, much larger than the parton size and the time scale of the current parton interactions. Then, during the time of interaction the parton can be regarded as quasifree, and the cross section calculated. In the string-parton model all string-string interactions are specified via effective parton-parton scattering and exchange. The probability that an interaction of two strings takes place has the form

$$W_{AB} \sim \rho_{i/A}(x_A)\rho_{j/B}(x_B)F_{ij}(\mathbf{b})\mathcal{P}_{ij},$$

where $\rho_{i/A}(x_A)$ denotes the probability density of finding a parton of type i with a given parton momentum fraction x_A in nucleon A . F_{ij} is the parton impact parameter dependence. $\mathcal{P}_{ij}(\theta)$ denotes the probability for scattering two partons with incoming momentum states p_i and p_j , and outgoing momentum states p_1 and p_2 , where θ is the angle between p_i and p_1 measured in the center-of-momentum frame of the partons. For a single parton-parton scattering, this probability has the t - and u -channel form as given by first-order perturbative QCD calculations [27], except here it is treated phenomenologically as

$$\mathcal{P}_{ij}(\theta) = \mathcal{A} \int_0^\theta d\theta' \left[\frac{s^2 + u^2}{(t - m_t^2)^2} + \frac{s^2 + t^2}{(u - m_u^2)^2} \right], \quad (2.4)$$

where \mathcal{A} is the normalization such that $\mathcal{P}_{ij}(\pi) = 1$. We sample this distribution with Monte Carlo techniques. The Mandelstam variables s , t , and u for the massless quarks are given by $s = 2p_i \cdot p_j$, $t = -2p_i \cdot p_1 = -s(1 - \cos\theta)/2$, and $u = -2p_i \cdot p_2 = -s(1 + \cos\theta)/2$. We use Monte Carlo techniques to obtain the distribution by randomly choosing \mathcal{P}_{ij} and inverting the equation to find θ . In practice we choose gluon masses $m_t = m_u = 0.25$ GeV which give a range of the interaction corresponding to the 30 mb pp inelastic cross section. The effective scattering results in a very different behavior in comparison to the simple Born scattering with zero

gluon mass. The effective scattering probability (2.4) includes the minijet terms in an average fashion. However, minijet phenomena are not expected to be significant at CERN energies. In order to preserve color neutrality, the gluon exchange is followed by a quark exchange [28]. The above interaction mechanism results in excitations of the strings due to the energy-momentum transfer. In nucleus-nucleus collisions all strings are allowed to interact with each other, including the strings produced by fragmentation as described below. In this sense multiple scattering effects are included in the dynamics of the evolution.

The real-time dynamics of interacting strings must be supplemented by a hadronization mechanism. Here, the string-parton model utilizes the pair creation followed by a string breakup method which is similar to flux-tube breaking of the strong-coupled QCD calculations [29]. Some experimental evidence is also provided by the studies of jets in e^+e^- and pp collisions. These experiments demonstrate that jets originate from hard quarks and gluons and provide support that fragmentation takes place within color neutral systems, and not from isolated partons [30].

In our simulation of high-energy collisions, string-string interaction mechanisms lead to excited strings which stretch and decay by breaking until they reach a predefined minimum mass. Each string may only decay into segments whose masses are above this cutoff mass. The minimum masses are $M_q = 0.28$ GeV for the mesonic strings, and $M_{qq} = 0.94$ GeV for baryon strings. The cutoff masses are determined by reproducing the correct hadron multiplicities and charge distributions in e^+e^- collisions [17]. We also note that the cutoff masses are just the minimum and, in practice, a spectrum of final string masses is produced (simulating excited states). The mass spectra obtained in the string-parton model correctly reproduce the observed distributions. The choice for the spatial decay point along the string is based on the invariant area decay law [31,32,17], in which the probability, \mathcal{P} , for a small segment of string to decay is a function of the invariant area it sweeps as it propagates, ΔA , and is given by $\mathcal{P} = 1 - \exp(-\Lambda\Delta A)$. The decay constant, Λ , could also be expressed in terms of a proper time interval for decay, $\Lambda = 1/\tau_0^2$, where $\tau_0 = 0.5$ fm/c which was fitted from μp collision data [18]. This simple decay law, combined with the string dynamics, produces many of the general features observed in high-energy fragmentation [17].

The pair-creation process is expected, not only to reproduce the longitudinal distributions observed in high-energy collisions, but also to contribute to the transverse momentum distributions. The quark and the antiquark of the created pair could carry equal and opposite nonvanishing transverse momenta. This source of transverse momenta will primarily contribute to the low momentum (approximately $p_T \leq 1.0$ GeV) part of the total transverse momentum distribution. In the absence of any fundamental calculations, we choose to parameterize the transverse momentum assignment with a simple exponential distribution function

$$f(p_T)p_T dp_T \propto e^{-\alpha p_T} p_T dp_T. \quad (2.5)$$

The assignment of p_T cannot exceed the available energy in the string, taking into account the cutoff masses. In practice we have used $\alpha = 3.88 \text{ GeV}^{-1}$ which accurately reproduces transverse momentum distributions in high-energy pp collisions [17]. The created quarks are initially virtual and become on shell by absorbing energy from the string. The virtual quarks may not interact until they become real; however, other quarks on the string are allowed to scatter as the string propagates. If the source of the transverse momentum is that acquired by the created virtual quarks, this directly influences the time taken by these particles to come on shell. This can simply be viewed as a manifestation of the Landau-Pomeranchuk effect.

III. COMPARISON WITH CERN HEAVY-ION DATA

We have applied the string-parton model to collision data for S+S, O+C, S+Al, and O+Au measured at NA35 [22] and WA80 [21] experiments at CERN. The collisions are followed to 100 fm/c in the collision frame, which is a sufficient amount of time for all particle production to have taken place.

The NA35 data which we have addressed are for S+S collisions in the impact parameter range $0 < b < 2.5 \text{ fm}$ at 200 A GeV [22]. In Fig. 1 the rapidity distributions are shown for all charged pions, and in Fig. 2 for the charged baryons. The important aspect of this data is that there has been some filling of the central rapidity region, but for the most part the baryons have not stopped. We can investigate this further by limiting the collision process, first by only allowing one collision per initial nucleon, then by allowing only baryon interactions, and finally by allowing all interactions. These results are shown in Fig. 3, where the rapidity distributions for the final baryons have been plotted. In order to facilitate comparisons for the case of one collision per nucleon, the curve has been normalized to the integrated particle number when all interactions are allowed. Notice that the central rapidity region fills when all baryon collisions are allowed, and that the filling is more pronounced when we allow

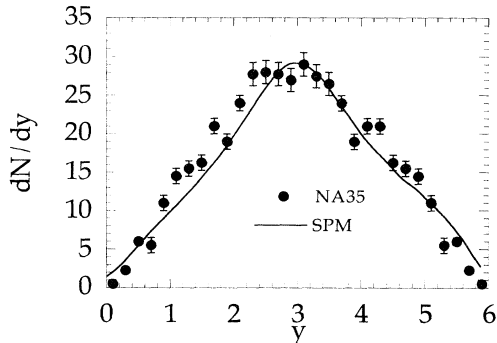


FIG. 1. Calculations of the charged pion rapidity distribution for S+S collisions (solid line). Experimental data are from NA35 [22] (dots). Details of the calculation are given in the text.

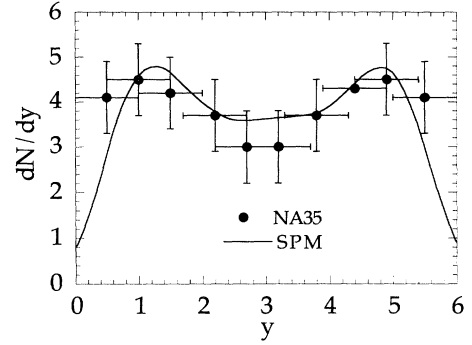


FIG. 2. Calculations of the charged baryon rapidity distribution for S+S collisions at 200 A GeV (solid line) compared to experimental data from NA35 [22] (dots). Details of the calculation are given in the text.

all collisions to occur. In Fig. 4 we show the behavior of the mesons for the same collision scenarios. Note that the central rapidity region fills as more collisions are allowed. We conclude from these calculations that multiple scattering of the baryons and mesons during the collision process is the principal cause for the Gaussian nature of the meson rapidity distributions, and the primary reason for the observed midrapidity nucleons.

We have also performed calculations to compare with data from WA80 [21] experiments. These experiments consider the transverse energy per unit of pseudorapidity produced in asymmetric collisions. We have investigated collisions of O+C and S+Al. The transverse energy is experimentally defined as

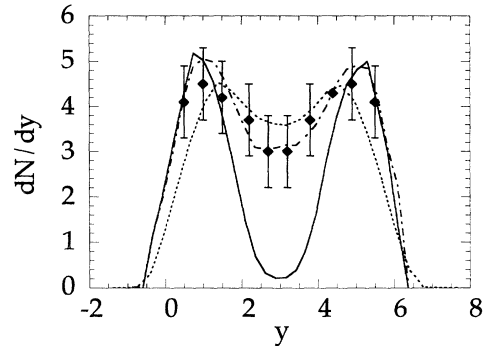


FIG. 3. Positive baryon rapidity distributions are shown for three interaction scenarios. In the first case (solid line) only one collision per incident nucleon is allowed, with no further interactions. In the second case (dotted line) all nucleon-nucleon interactions are allowed. This increases the total number of interacting nucleons. More nucleons are found in the central regions, and the leading baryons have lost approximately one unit of rapidity. In the final case all nucleon-nucleon, pion-nucleon, and pion-pion interactions are allowed (dash-dotted line), from which further enhancements of the midrapidity baryons and a further rapidity loss of the leading baryons is also observed.

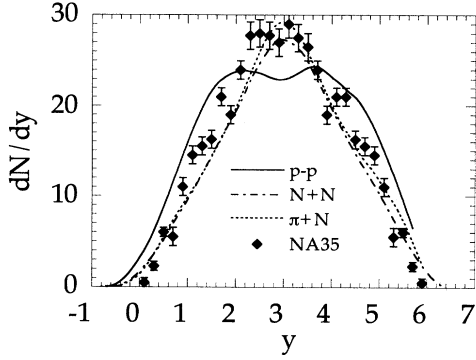


FIG. 4. Negative hadron rapidity distributions are shown for three interaction scenarios, as described in Fig. 3. More mesons are found in the central regions as further collisions are allowed.

$$E_T = \int d\eta \frac{dE_T}{d\eta}, \quad (3.1)$$

$$= \int d\eta \sum_{i=1}^M E_i \sin \theta_i \delta(\eta - \eta_i), \quad (3.2)$$

where, for a given particle i , the transverse energy is $E_T = E_i \sin \theta_i$, and θ_i is the angle between particle i and the beam axis. Cuts on the experimental data are made by considering only pseudorapidities in the range $2.4 < \eta < 5.5$, and requiring that the ratio of the total energy deposited in the forward calorimeter, E_F (at $\eta > 6.0$), to the total transverse energy in any collision is

$$\frac{E_F}{E_{\text{beam}}} \leq 0.88. \quad (3.3)$$

We show for the O+C and S+Al systems the transverse energy spectra in Fig. 5. Total cross sections are calculated through the formula

$$\sigma_{\text{tot}} = \pi R^2 \frac{N}{N_T}, \quad (3.4)$$

where N is the total number of collisions that satisfy

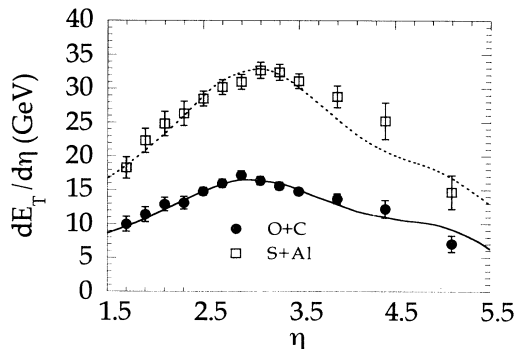


FIG. 5. The transverse energy of all hadrons is shown for the O+C and S+Al systems. Calculations are given by the lines, while experimental WA80 data [21] are shown by the symbols listed on the figure.

the trigger cut of Eq. (3.3), N_T is the total number of Monte Carlo collisions, and $R = R_1 + R_2 + \delta$ is the radius of the collision area, with R_i being the radius of either nuclei, and $\delta = 1.0$ fm. In Fig. 6 we show the cross section $d\sigma/dE_T$ as a function of E_T for the O+C and S+Al systems.

IV. DYNAMICAL ENERGY DENSITIES

As a fully dynamical theory, the string-parton model can be used to study the time evolution of the meson energy density produced in relativistic nucleus-nucleus collisions. Several procedures may be used to calculate the central energy density. For example, the quark-gluon string model counts all hadrons, including those not yet formed, in energy density calculations [13]. Thus, this calculation obtains significant energy densities for 160A GeV Pb+Pb collisions ($20 \text{ GeV}/\text{fm}^3$ at a time of $t=1.05 \text{ fm}/c$). The VENUS model calculates the energy density with on-shell hadrons, using the “rather arbitrary definition of the hadronization point which is defined as the point where two corresponding (produced) partons meet” for the first time [33]. VENUS calculations obtain $\varepsilon_{\text{max}} \sim 4 \text{ GeV}/\text{fm}^3$ for 200A GeV O+Au collisions. The time scale to this maximum density was $\tau \sim 1.0 \text{ fm}/c$, which is expected since $\tau \propto \kappa$ in this calculation.

In our calculations of the central energy densities we will consider only produced on-shell mesons. Although this is in the spirit of the calculations of Ref. [33], several differences are explained by the different time scales involved in the problem, and of the dynamics of our decay mechanism, as discussed below. Calculations are performed in the center-of-momentum frame of the produced mesons. In this frame the maximal longitudinal extent of the volume, ℓ , is determined by the separation of the two leading nuclei from the time of their initial contact. This length is $\ell = 2\beta(t - t_0)$, where t_0 is the initial time of contact, and β is the velocity of the leading baryons. The energy and number densities for a radial shell of area $2\pi r dr$ are then given by $\varepsilon(r) = E(r)/(2\pi r dr \ell)$ and $n(r) = N(r)/(2\pi r dr \ell)$, where $E(r)$ and $N(r)$ are the energy and number of mesons contained in the shell. The transverse extent of the volume is obtained by sampling

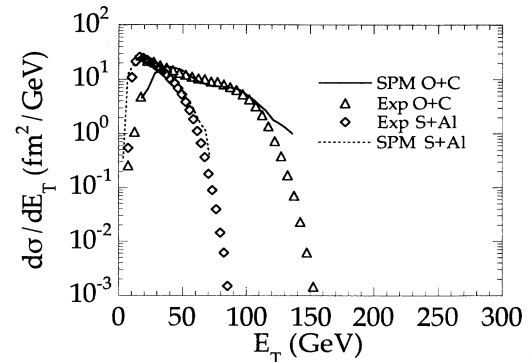


FIG. 6. The differential cross section $d\sigma/dE_T$ is plotted as a function of E_T for the O+C and S+Al systems.

the radial meson distribution, $N(r)$. The meson number and energy densities at a given time are then

$$\langle \epsilon \rangle = \frac{\int N(r)\epsilon(r)d^2r}{\int N(r)d^2r}, \quad \langle n \rangle = \frac{\int N(r)n(r)d^2r}{\int N(r)d^2r}. \quad (4.1)$$

The calculation of the energy density is primarily influenced by various time scales involved in hadroproduction. These time scales include the interaction time, i.e., the time taken for the two nuclei to cross each other, the decay or excitation time, and the time required for the created virtual mesons to become on shell. The model correctly reproduces the experimental transverse energy spectra, shown in the previous section, which is the quantity used in the Björken formula for predicting the central energy density. For S+S collisions the ratio of baryons to mesons in the central rapidity region is on the order of 5% [22]. Thus they do not contribute significantly to the measured transverse energy spectrum, $dE_T/d\eta$.

In Fig. 7(a) we show the time dependence of the meson energy density for 200A GeV O+O, S+S, and Cu+Cu collisions at zero-impact parameter. We note that the maximum energy density in the central region scales

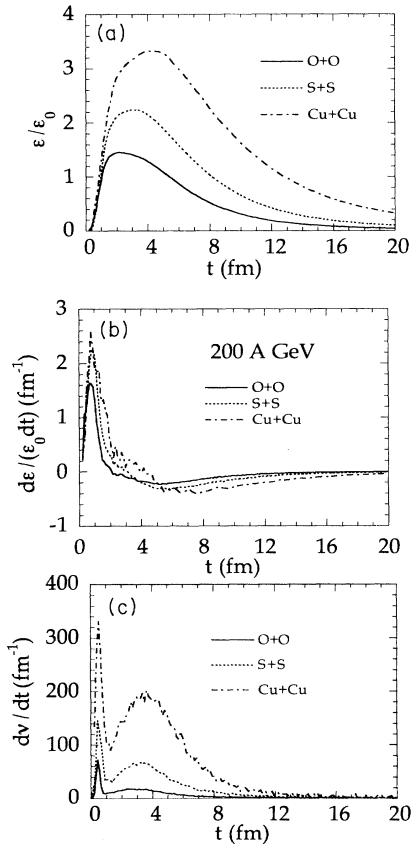


FIG. 7. (a) The central meson energy density, defined in the text as a function of time, is plotted for O+O, S+S, and Cu+Cu collisions at 200A GeV. (b) The time derivative of the energy density is shown for the two systems. (c) The collision rate dv/dt is shown for the two systems. In (b) and (c) the derivatives are numerical.

roughly as $A^{0.62}$. Statistical fluctuations in the radial number density, $N(r)$ are on the order of 40%. For the Cu+Cu collisions we also considered central slabs of widths 1.0, 2.0, and 3.0 fm, and found insignificant differences with the maximum central energy density obtained as described above. Results of these slab calculations are given in Fig. 8. We have also checked that slices in rapidity about $y = 0$ alter the results by only 10–20%. Inclusion of baryons in the central region, ($|y| < 0.5$), increases the energy density by 10%. We have also made calculations for determining the beam energy dependence of the meson energy density. We find a dependence which roughly scales as $\ln \gamma$. These results predict an approximately 2.9 GeV/fm³ meson energy density for U+U at 100A GeV collider energy. We also note the $1/t$ dependence of the meson energy density at large times. In Fig. 7(b) we show the time derivative of the scaled meson energy density, $d(\epsilon/\epsilon_0)/dt$, where $\epsilon_0 = 0.16$ GeV/fm³, which is the energy density in infinite nuclear matter. We also show in Fig. 7(c) the collision rate, dv/dt . An overview of the collision becomes quite clear as we view Fig. 7. For example, for the S+S system the two nuclei begin to overlap at 0 fm/c, as indicated by the onset of collisions at that time. By approximately 0.5 fm/c, the two nuclei are completely overlapping and particle production has begun, as shown by the dm/dt curve. At 1.0 fm/c the energy production rate has reached its maximum, as indicated in Fig. 7(b). Secondary collisions of baryons and mesons are indicated by the broad peak of dv/dt at 3.0 fm/c. The maximum meson mass density appears at roughly the same time as can be seen in Fig. 7(a). Note that there are many more secondary collisions in the S+S system. These collisions are actually occurring in the baryon-rich regions. Maximum values of the energy density also depend on the number of nucleons involved in the collision. We show in Fig. 9 (right ordinant) the A dependence of the energy density for the O, S, and Cu collisions at 200A GeV. The energy density scales as $(\epsilon/\epsilon_0)_{\max} = 0.28A^{0.6}$.

String-parton model calculations of the maximum en-

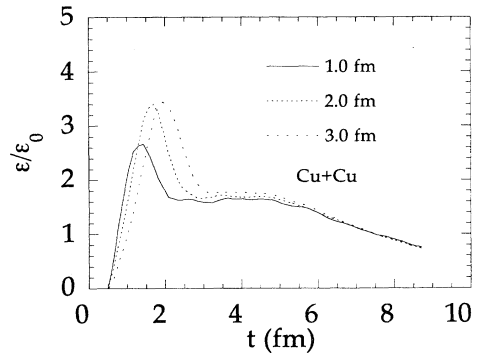


FIG. 8. The central density in a longitudinal slab in the central region of thickness 1.0, 2.0, and 3.0 fm is shown as a function of time for Cu+Cu at 200A GeV. Note that the maximum density obtained using these constant longitudinal slabs is not significantly different from the full longitudinal expansion given in Fig. 7(a).

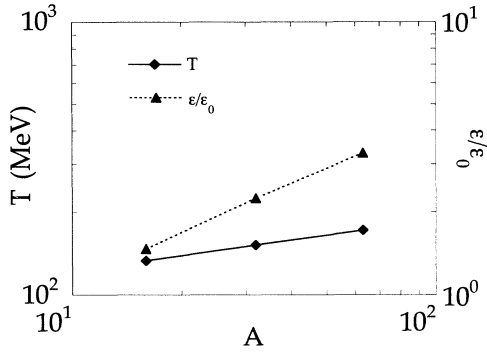


FIG. 9. For the systems O+O, S+S, and Cu+Cu at 200A GeV and zero-impact parameter, we show the A dependence of the maximum energy density (right ordinate), and the temperature (left ordinate).

ergy density for mesons formed during nuclear collisions are smaller than the densities given by estimates obtained from the Bjørken formula [21] by factors of 3 to 4, depending on the nuclear system involved. These estimates are calculated using the Bjørken energy density formula [34]

$$\varepsilon_{Bj} = \frac{dE_T/d\eta|_{\max}}{\pi R_0^2 \tau}, \quad (4.2)$$

where πR_0^2 is the transverse area of the smaller of the two colliding nuclei, and τ is taken to be 1 fm/c, which is the assumed longitudinal extent of the volume at maximum energy density. This formula is based on the assumption of longitudinal rapidity scaling which is not supported by the data at SPS energies [21] or by the NA35 data presented above. The Bjørken formula does not take into account the finite size of the nucleus nor the nuclear collision times. Furthermore, the time scale used in the formula is taken to be the strong interaction time, 1 fm/c, which does not account for the time required for the virtual particles to become on shell.

A modified form of the Bjørken estimate, which takes into account the interaction times, t_I , and formation times, t_H , can be used to reproduce the results obtained from the string-parton model. The modified Bjørken energy density is given by

$$\hat{\varepsilon} = \frac{dE_T/d\eta|_{\max}}{\pi R^2 2\beta t}, \quad (4.3)$$

where $t = t_I + t_H$, and R is the transverse rms radius of

the pion source at maximum energy density. The factor $2\beta t$ gives the longitudinal extent of the volume, and is calculated as discussed in a preceding paragraph. The collision time is associated with the time of overlap of the two nuclei, which for central collisions is calculated in the center-of-momentum frame from the formula

$$t_I = \left(\frac{2R_1}{\gamma_1} + \frac{2R_2}{\gamma_2} \right) \frac{1}{|\beta_1| + |\beta_2|}, \quad (4.4)$$

where 1 and 2 correspond to nucleus 1 or 2. In the case of varying impact parameters, we average the radii over impact parameter. The initial meson formation time—the time interval between nuclear overlap and the maximum energy density—is determined by the sum of an initial decay time, secondary scatterings, and the time required for the virtual quarks to become on shell. We list in Table I, for various nuclear systems, t_I , calculated from Eq. (4.4), and the total time, t , to maximum density, ε_{\max} , calculated from the string-parton model. We also show the unmodified Bjørken energy density, ε_{Bj} , obtained from experimental data using $\tau = 1$ fm/c, and the modified energy density calculation $\hat{\varepsilon}$.

V. THE THERMODYNAMIC EVOLUTION OF THE PRODUCED MESONS

Mesons produced during the collision process may be investigated in terms of the thermodynamics of a relativistic boson gas of noninteracting particles. Although these assumptions are frequently made to extract thermodynamic information from data their validity is not well established. The present heavy-ion data does not show a bosonic distribution for the produced particles. For this reason the interpretation of this analysis should be done with caution. However, our results can be compared with those calculations that make the same assumptions [35]. We have checked that in the central region there are a few secondary collisions, and that most of these collisions occur near the leading nuclear fragments. We have assumed that the produced mesons may be mapped onto an ensemble of noninteracting pions at each instant of time, and thus, we may calculate a temperature and chemical potential for these particles.

We base our thermodynamic calculations on the grand canonical partition function, and we assume that at each time during the collision one can treat the produced particles as a noninteracting distribution. We employ the grand canonical ensemble

TABLE I. A comparison of various time scales and central energy densities for a number of collisions at 200A GeV. Time units are in fm/c, and energy densities are given in GeV/fm³. The radii at maximum energy density, R , are given in fm. The O+C calculation was performed for midimpact parameters as defined in WA80 experiments. Statistics for O+Au allow for only single-digit precision.

System		R	t_I	t	ε_{\max}	ε_{Bj}	$\hat{\varepsilon}$
O+C		2.3	0.21	2.2	0.20	0.7 [11]	0.19
O+O	($b = 0$)	2.6	0.59	2.3	0.27		0.24
S+S	($b = 0$)	3.2	0.74	3.1	0.36		0.34
O+Au	($b = 0$)	3.8	0.97	4.3	0.3	2.2 [11]	0.3

$$Z_G = \text{Tr} \left\{ \exp \left[-\beta \left(\hat{H} - \mu \hat{N} \right) \right] \right\}, \quad (5.1)$$

for a gas of noninteracting pions, where μ is the chemical potential and T is the temperature of the system, such that $\beta = 1/T$. We assume a noninteracting Hamiltonian, $\hat{H}\psi = E\psi$, whose occupation number operator is given by \hat{N} . The thermodynamic potential $\Omega(T, V, \mu)$, where V is the volume of the system, is related to the grand partition function by

$$\Omega(T, V, \mu) = -T \ln Z_G,$$

and the density operator for the system is

$$\hat{\rho}_G = Z_G^{-1} \exp \left[-\beta \left(\hat{H} - \mu \hat{N} \right) \right].$$

Thus for any operator \hat{O} we can calculate the expectation value by performing the trace

$$\langle \hat{O} \rangle = \text{Tr} \left(\hat{\rho}_G \hat{O} \right). \quad (5.2)$$

For our boson gas we may calculate the grand partition function in occupation number Hilbert space from Eq. (5.1)

$$Z_G = \prod_{i=1}^{\infty} \text{Tr}_i \exp \left[-\beta (e_i - \mu) \hat{n}_i \right],$$

where \hat{n}_i is the single-particle occupation number operator. For bosons, the occupation numbers are unrestricted so we sum n_i over all integrals to obtain

$$Z_G = \prod_{i=1}^{\infty} [1 - \exp \beta (\mu - e_i)]^{-1}. \quad (5.3)$$

In terms of the grand partition function the thermodynamic potential becomes

$$\Omega_0(T, V, \mu) = -T \sum_{i=1}^{\infty} \ln \{1 - \exp[-\beta(\mu - e_i)]\}. \quad (5.4)$$

We use a relativistic dispersion for the energy of a particle, $e_p = \sqrt{p^2 + m^2}$, and apply periodic boundary conditions to the single-particle wave functions. This allows us to go from sums in particle numbers to integrals in momentum space:

$$\sum_{i=1}^{\infty} \rightarrow \frac{4\pi g^3}{2\pi\hbar^3} \int \sqrt{e^2 - m^2} e d e, \quad (5.5)$$

where m is the particle mass, and g is the degeneracy factor ($g = 3$ for pions).

Using Eq. (5.2), we extract a temperature and chemical potential through the relations

$$\langle \epsilon \rangle = \frac{g}{2\pi^2 \hbar^3} \int \sqrt{e^2 - m^2} e^2 f(\mu, T) d e, \quad (5.6)$$

$$\langle n \rangle = \frac{g}{2\pi^2 \hbar^3} \int \sqrt{e^2 - m^2} e f(\mu, T) d e, \quad (5.7)$$

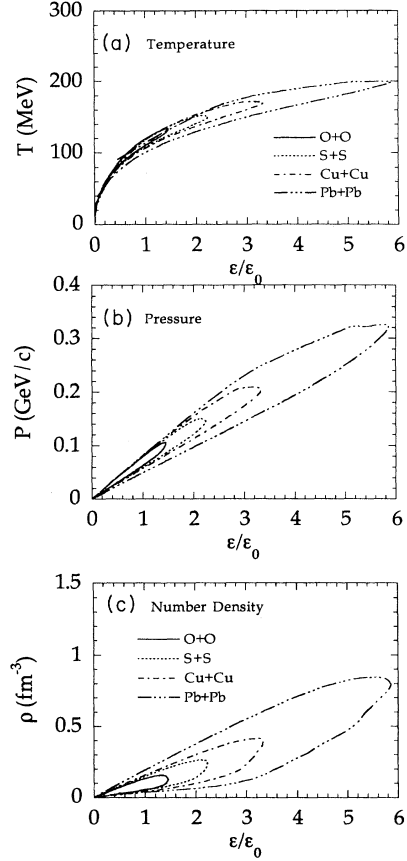


FIG. 10. Thermodynamic quantities are plotted as a function of the scaled energy density for O+O and S+S at 200A GeV, and Pb+Pb at 160A GeV. In each case, time moves in the clockwise direction. The temperature (a), pressure (b), and number density (c) are plotted, with $\epsilon_0 = 0.16 \text{ GeV}/\text{fm}^3$.

where $m = 0.35 \text{ GeV}$ is the average meson mass in the string calculation. In order to obtain an estimate for the temperature and chemical potentials of the system, we use the distribution $f(\mu, T) = 1/\{1 - \exp[(e - \mu)/T]\}$. The thermodynamic pressure may be calculated in a similar fashion. We use the energy and number densities

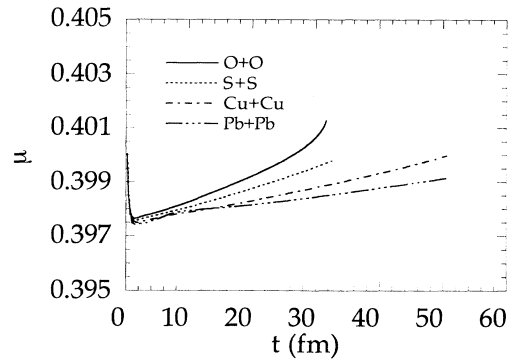


FIG. 11. The chemical potential is shown for the collisions of O+O, S+S, and Cu+Cu at 200A GeV, and Pb+Pb at 160A GeV.

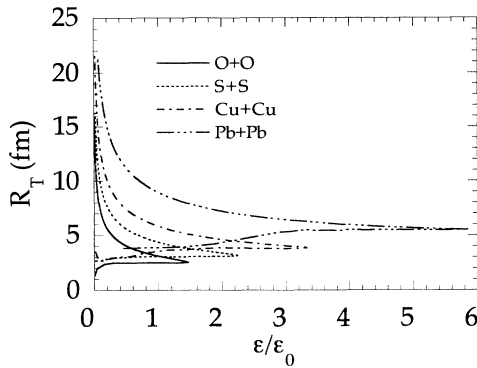


FIG. 12. The rms transverse radius of the pion gas is shown for the collisions of O+O, S+S, and Cu+Cu at 200A GeV, and Pb+Pb at 160A GeV.

calculated from the string parton model and extract a chemical potential and temperature from the nonlinear set of equations (5.6) and (5.7).

The thermodynamic evolution of the produced mesons for the various systems we have studied is shown in Fig. 10. In all cases measurements were taken every 0.135 fm/c, and time moves in the clockwise direction. We have shown in Fig. 10(a) the temperature, in Fig. 10(b) the pressure, and in Fig. 10(c) the meson number density as a function of ϵ/ϵ_0 . The chemical potential is roughly a constant throughout the calculation at $\mu = 0.4$ GeV, as shown in Fig. 11. We also show the evolution of the transverse radius as a function of ϵ/ϵ_0 in Fig. 12. These calculations show that the thermodynamics from smaller systems to the larger systems is smooth, and does not exhibit discontinuities in any variables.

In Fig. 9 (left ordinant) we show the A dependence of the temperature for the various systems we studied. The temperature scales as $T = 80A^{0.18}$ MeV. We do not include the Pb collision here since the calculation was performed at 160A GeV. We also show in Fig. 13 the scaling of maximum temperature with maximum energy density. The scaling is given by $T = 119(\epsilon/\epsilon_0)^{0.3}$ GeV, where the Pb collision has been included.

VI. CONCLUSIONS

We have presented in this paper a dynamical model in 3+1 dimensions for the evolution of hadronic matter in relativistic collision, and we have applied this model to various physical systems for which there is experimental data. We found that, in general, the string-parton model is able to reproduce the experimental data that characterize average hadronic quantities. We noted that the filling in of the central rapidity distribution in S+S experimental data (NA35) is due to rescattering effects. From our energy density calculations, we were able to propose a modified version of the Bjorken energy density which takes into account both the interaction time for nuclear overlap, and the formation times involved with pair production. The issues related to the various time scales involved in the hadronization and particle produc-

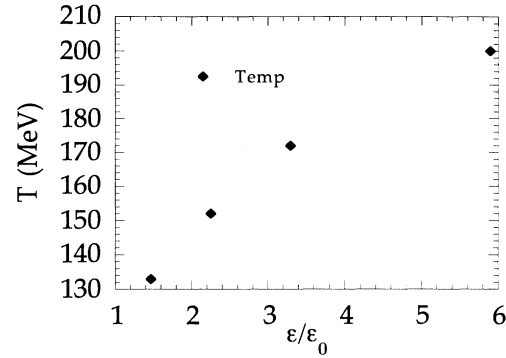


FIG. 13. For the zero-impact parameter collisions of the systems O+O, S+S, and Cu+Cu, each at 200A GeV, and Pb+Pb at 160A GeV, the energy dependence of the temperature is plotted as a function of the temperature.

tion processes require more theoretical discussions and a better understanding of the underlying dynamics of these processes. However, it is clear that the additional time delay in our model necessarily leads to a lower-energy density. For QED based complex reactions the physical outcome is very clear; only a fraction of the energy density can be reconstructed from the produced lepton pairs even though the QED field energy density can be very large. Thus, it is clearly advantageous to search for the signature of the quark-gluon plasma formation rather than infer it from inclusive hadronization data. We have also used the thermodynamics of a relativistic gas of non-interacting pions to estimate the temperature and other thermodynamic quantities. We used the calculated energy and particle densities from the string-parton model as input to these calculations. All of the thermodynamic calculations indicate a smooth transition in temperature, energy density, and meson number density. The string-parton model can only address average hadronic quantities, and it has been shown in this paper that these quantities vary smoothly as one increases the mass of the colliding nuclei. An important caveat to stress is that the string-parton model does not contain mechanisms for the transition from hadronic matter to the quark-gluon plasma. At higher energies, strong correlations may drive the system to a much different energy density and temperature than that based on purely hadronic degrees of freedom. We anticipate in the future to continue these calculations at RHIC energies.

ACKNOWLEDGMENTS

This research was sponsored in part by the U.S. Department of Energy under Contract No. DE-AC05-84OR21400 managed by Martin Marietta Energy Systems, Inc., and under Contract No. DE-FG05-87ER40376 with Vanderbilt University. The numerical calculations were carried out on CRAY-2 supercomputers at the National Center for Supercomputing Applications, Champaign, Illinois, at the National Energy Research Supercomputer Center, Livermore, and on the Intel iPSC/860 hypercube at the Oak Ridge National Laboratory.

- [1] *Proceedings of Quark Matter '91*, edited by T. C. Awes, F. E. Obenshain, F. Plasil, M. R. Strayer, and C. Y. Wong [Nucl. Phys. **A544** (1992)].
- [2] A. Ukawa, Nucl. Phys. **A498**, 227c (1989); M. Fukugita, S. Ohta, Y. Oyanagi, and A. Ukawa, in *Field Theory on the Lattice*, Proceedings of the International Symposium, Seillac, France, 1987, edited by H. Billoire [Nucl. Phys. **B**, Proc. Suppl. **4**, 105 (1988)]; Phys. Rev. Lett. **58**, 2515 (1987); J. B. Kogut, J. Polonyi, H. W. Wyld, and D. K. Sinclair, Phys. Rev. D **31**, 3304 (1985).
- [3] S. Gottlieb, W. Liu, D. Toussaint, R. L. Renken, and R. L. Sugar, Phys. Rev. Lett. **59**, 1513 (1987); **59**, 1881 (1987), **59**, 2247 (1987); Phys. Rev. D **38**, 2888 (1988); C. DeTar and J. Kogut, Phys. Rev. Lett. **59**, 399 (1987); Phys. Rev. D **36**, 2828 (1987); T. A. DeGrand and C. E. DeTar, *ibid.* **34**, 2469 (1986).
- [4] F. R. Brown, F. P. Bulter, H. Chen, N. H. Christ, Z. Dong, W. Schaffer, L. I. Unger, and A. Vaccarino, Phys. Rev. Lett. **65**, 2491 (1990); M. Fukugita, H. Mino, M. Okawa, and A. Ukawa, Phys. Rev. Lett. **65**, 816 (1990); P. F. Hsieh, Phys. Rev. D **43**, 3475 (1991).
- [5] G. E. Brown, H. A. Bethe, and P. M. Pizzochero, Phys. Lett. B **263**, 337 (1991).
- [6] C. Baglin *et al.*, Phys. Lett. B **220**, 471 (1989).
- [7] J. Bartke *et al.*, NA35 Collaboration, Z. Phys. C **48**, 200 (1990).
- [8] J. Schukraft, CERN Report No. CERN-PPE/91-04, 1991.
- [9] B. Müller, in [1], p. 95c.
- [10] B. Andersson and G. Gustafson, Z. Phys. C **3**, 223 (1980); B. Andersson, G. Gustafson, G. Ingelman, and T. Sjöstrand, Phys. Rep. **97**, 33 (1983).
- [11] B. Andersson, G. Gustafson, and B. Nilsson-Almqvist, Nucl. Phys. **B281**, 289 (1987).
- [12] K. Werner, Z. Phys. C **42**, 85 (1989).
- [13] N. S. Amelin, E. F. Staubo, L. P. Csernai, V. D. Toneev, K. K. Gudima, and D. Strottman, Phys. Lett. B **261**, 352 (1991).
- [14] H. Sorge, A. v. Keitz, R. Mattiello, H. Stöcker, and W. Greiner, Z. Phys. C. **47**, 629 (1990).
- [15] E. F. Staubo, A. K. Holme, L. P. Csernai, M. Gong, and D. Strottman, Phys. Lett. B **229**, 351 (1991); J. Rentsch, G. Graebner, J. A. Maruhn, H. Stöcker, and W. Greiner, Mod. Phys. Lett. **2**, 193 (1987).
- [16] K. Geiger and B. Müller, Nucl. Phys. **B369**, 600 (1992).
- [17] D. J. Dean, Ph.D. thesis, Vanderbilt University, 1991 (unpublished); D. J. Dean, A. S. Umar, J.-S. Wu, and M. R. Strayer, Phys. Rev. C **45**, 400 (1992); D. J. Dean, A. S. Umar, J.-S. Wu, and M. R. Strayer, in *Proceedings of Computational Quantum Physics*, edited by A. S. Umar, V. E. Oberacker, C. Bottcher, and M. R. Strayer, AIP Conf. Proc. No. 260 (AIP, New York, 1992), p. 159.
- [18] A. S. Umar, D. J. Dean, and M. R. Strayer, in [1], p. 475c.
- [19] D. J. Dean, M. Gyulassy, B. Müller, E. A. Remler, M. R. Strayer, A. S. Umar, and J.-S. Wu, Phys. Rev. C **46**, 2066 (1992).
- [20] D. J. Dean, A. S. Umar, and M. R. Strayer, Int. J. Mod. Phys. E (in press, 1993).
- [21] R. Albrecht *et al.*, WA80 Collaboration, Phys. Rev. C **44**, 2736 (1991).
- [22] H. Ströbele *et al.*, NA35 Collaboration, Nucl. Phys. **A525**, 59c (1991).
- [23] X. Artru, Phys. Rep. **97**, 147 (1983).
- [24] V. D. Barger and R. J. N. Phillips, *Collider Physics* (Addison-Wesley, New York, 1987), and references therein; P. D. B. Collins and A. D. Martin, *Hadron Interactions* (Adam Hilger, Bristol, 1984).
- [25] T. Sloan, G. Smadja, and R. Voss, Phys. Rep. **162**, 45 (1988).
- [26] A. Bodek *et al.*, Phys. Rev. D **20**, 1471 (1979).
- [27] R. Cutler and D. Sivers, Phys. Rev. D **17**, 196 (1978).
- [28] N. Isgur, Nucl. Phys. **A497**, 91c (1989); K. Maltman and N. Isgur, *ibid.* **29**, 952 (1984).
- [29] R. Kokoski and N. Isgur, Phys. Rev. D **35**, 907 (1987); G. A. Müller, *ibid.* **37**, 2431 (1988); P. Geiger and N. Isgur, *ibid.* **41**, 1595 (1990).
- [30] P. Mättig, Phys. Rep. **177**, 141 (1989).
- [31] K. Sailer, B. Müller, and W. Greiner, J. Mod. Phys. A **4**, 437 (1989); K. Sailer, B. Müller, and W. Greiner, in *Proceedings of The Nuclear Equation of State*, edited by W. Greiner and H. Stöcker (Plenum, New York, 1990), p. 531.
- [32] E. A. Remler, *Proceedings of XXXI Cracow School of Theoretical Physics* (Zakopane, Poland, 1991); E. A. Remler, Proceedings of the International Workshop on Quark-Gluon Structure of Hadrons and Nuclei, Shanghai, 1990 (unpublished); E. A. Remler, College of William & Mary report, 1988 (unpublished); E. A. Remler, Proceedings of the Gross Properties of Nuclei and Nuclear Excitations, Hirschegg, 1987 (unpublished), p. 24.
- [33] K. Werner, Phys. Lett. B **219**, 111 (1989).
- [34] J. D. Björken, Phys. Rev. D **27**, 140 (1983).
- [35] D. P. Menezes, F. S. Navarra, M. Nielsen, and U. Ornik, Phys. Rev. C **47**, 2635 (1993); J. Boltz, U. Ornik, and R. M. Weiner, *ibid.* **C47**, 1738 (1993); E. Schnedermann and U. Heinz *ibid.* **47**, 1738 (1993).